Direct mapping of cytomechanical homeostasis destruction in osteoarthritis based on silicon nanopillar array

Dengjie Yu, Qingbin Nie, Jiangtao Xue, Ruizeng Luo, Shiwang Xie, Shengyu Chao, Engui Wang, Linlin Xu, Yizhu Shan, Zhuo Liu[*], Yusheng Li[*], Zhou Li[*]

D. Yu, Y. Li

Department of Orthopedics, Xiangya hospital, National Clinical Research Center for Geriatric Disorders, Xiangya hospital, Central South University, Changsha, 410008, China

E-mail: liyusheng@csu.edu.cn

D. Yu, J, Xue, R. Luo, S. Xie, S. Chao, E. Wang, L. Xu, Y. Shan, Z. Liu, Z. Li

Beijing Institute of Nanoenergy and Nanosystems, Chinese Academy of Sciences, Beijing, 101400, China.

E-mail: zli@binn.cas.cn

Z. Liu

Key Laboratory of Biomechanics and Mechanobiology, Ministry of Education, Beijing Advanced Innovation Center for Biomedical Engineering, School of Engineering Medicine, Beihang University, Beijing 100191, China.

E-mail: liuzhuo@buaa.edu.cn

Q. Nie

Department of Neurosurgery, PLA General Hospital, Beijing, 100853, China.

Z. Li

Institute for Stem Cell and Regeneration, Chinese Academy of Sciences, Beijing 100101, China.

J. Xue

School of Medical Technology, Beijing Institute of technology, Beijing, 100081, China.

L. Xu

CAS Key Laboratory for Biomedical Effects of Nanomaterials and Nanosafety & CAS Center for Excellence in Nanoscience, National Center for Nanoscience and Technology of China, Beijing 100190, Beijing, China.

Abstract

WILEY-VCH

Osteoarthritis (OA) is the most prevalent joint degenerative disease characterized by chronic joint inflammation. The pathogenesis of OA has not been fully elucidated yet. Cartilage erosion is the most significant pathological feature in OA, which is considered as the result of the cytomechanical homeostasis destruction. The cytomechanical homeostasis is maintained by the dynamic interaction between cells and the extracellular matrix, which can be reflected by cell traction force (CTF). It is critical to assess the CTF for providing a deeper understanding of the cytomechanical homeostasis destruction and progression in OA. In this study, a silicon nanopillar array (Si-NP) with high spatial resolution and aspect ratio is fabricated to investigate the CTF in response to OA. We discover the CTF is degraded in OA, which is attributed to the F-actin reorganization induced by the activation of RhoA/ROCK signaling pathway. Si-NP also show promising potential as a mechanopharmacological assessment platform for OA drug screening and evaluation.

1. Introduction

Osteoarthritis (OA) is the most prevalent joint degenerative disease, with a rate of 8%–10% in all age groups and reaching 70% in people aged > 70 years.[1] The prevalence of OA has increased by 107 over the past three decades and it continues to increase as the population ages.[2] Osteoarthritis is characterized by chronic inflammation of affected joints that causes pain that leads to a loss of mobility and structural changes. Over the course of the disease, a significant proportion of individuals will become disabled, resulting in a decreased quality of life and demand for surgical intervention.[3] The high prevalence and severity have imposed a serious threat to individual health and socioeconomies.[4] However, the pathogenesis and mechanisms of OA remain unclear, restricting its early diagnosis and treatment.

Chondrocytes are the sole cell type in cartilage tissues. After OA is initiated, an imbalance between anabolic and catabolic events in chondrocytes leads to several symptoms, including cartilage erosion, systemic inflammation, and subchondral bone remodeling (Figure 1a).[5] Among these processes, cartilage erosion is one of the most significant pathological features of OA; it causes progressive mechanical degradation and eventually leads to cartilage loss, which is the onset of structural destruction in the joint and disease progression.[6] Understanding of the OA mechanism has deepened, and cartilage erosion is now regarded as a spontaneous mechanical degradation process

WILEY-VCH

induced by chronic OA inflammation, instead of mechanical breakdown caused by external forces.[7] Tissue mechanical properties are virtually an integration of cellular mechanics that are maintained by dynamic interaction between cells and their mechanical environment, which is the extracellular matrix (ECM)[8] where resident cells serve as the mechanical foundation of the tissues. The composition and structure of the ECM are determined and regulated by the dynamics of these cells.[9] They sense and respond to the mechanical microenvironment through focal adhesions (FA) and the cytoskeleton. Focal adhesions comprise an integration of transmembrane proteins that link the ECM and the intracellular cytoskeleton, then detect and transmit mechanical signals into cells.[10] These signals are subsequently transmitted through the cytoskeleton to the nucleus, where they induce mechanical deformation of its structure, resulting in transcriptional regulation. The constituents and structure of the ECM are transcriptionally regulated to maintain stability in the mechanical microenvironment through dynamic interactions between cells and the ECM; this is termed cytomechanical homeostasis.[11] In turn, contractile reaction force exerted by cells onto the ECM through focal adhesions (FAs) and cytoskeleton is defined as cell traction force (CTF). This plays a significant role in many physiological processes, such as adherence, migration, and proliferation.[12] However, although cellular mechanical destruction is a known response to OA,[13] the response of cytomechanical homeostasis in OA as a maintenance factor for mechanical properties, remains unknown. Therefore, assessment of CTF in response to OA is essential to provide a deeper understanding of the cytomechanical homeostasis response and the process of cartilage erosion in OA.

We fabricated a silicon nanopillar array (Si-NP) for CTF assessment using electron beam photolithography (EBL) (**Figure** 1b and c). These Si-NPs had high spatial resolution and a high aspect ratio, which enabled reliable and precise CTF measurements.[14] We used silicon because its solid and rigid mechanical properties avoid collapse and substrate interference.[15] We attributed CTF degradation in response to OA to RhoA/ROCK activation-induced F-actin reorganization based on the Si-NPs. Our findings provide new insight into the mechanotransduction process in OA and might help to better understand the destruction of cytomechanical homeostasis that leads to cartilage erosion and the development of OA at the cellular level. Furthermore, Si-NPs showed potential as a high-throughput mechanopharmacological assessment platform for OA drug screening when OA was treated with drugs targeting different factors in the clinical settings (**Figure** 1d).
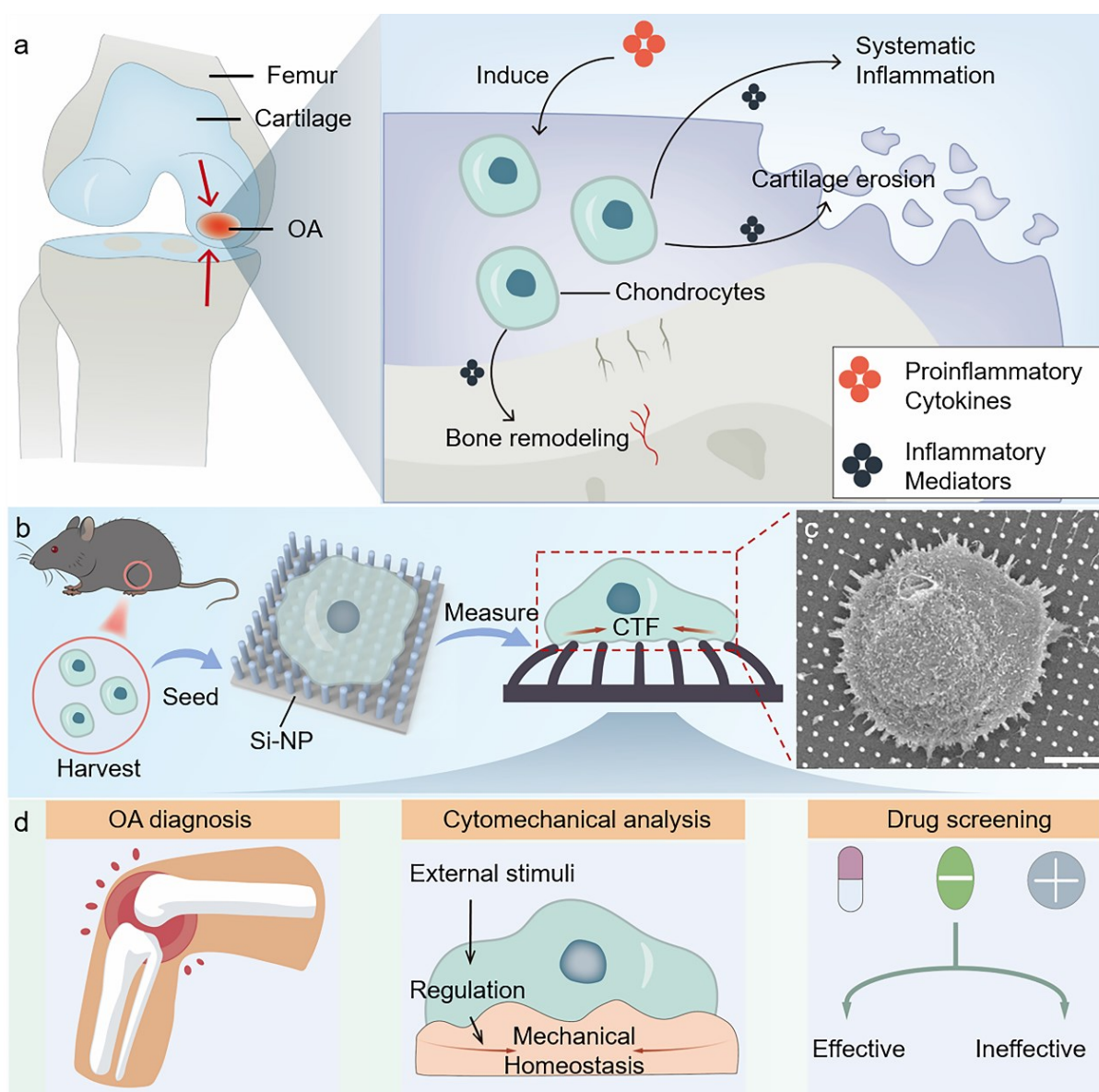
4

Figure 1. Illustration of CTF assessment in response to OA. (a) Schematic illustration of the pathogenesis of OA. (b) The process for chondrocyte CTF assessment. (c) SEM image of a chondrocyte seeded on the Si-NP (scale bar, 4μm). (d) Intended applications of the Si-NP.

2. Results and discussion

2.1. Fabrication and characterization of Si-NP

A reliable measurement platform is required to ensure a precise CTF assessment. The greatest advantage of nanopillars over deformable microbeads is that the CTF at each position can be measured independently.[16] However, pillar collapse, substrate interference, and low spatial resolution are major problems for nanopillars based on organic materials that all lead to errors between readouts and a realistic CTF.[17] Silicon has been used to fabricate nanopillar arrays because of its rigidity (Young modulus, 150 GPa) and processability. The parameters of the silicon nanopillars were adjusted based on EBL and on the demand for a high-resolution optical readout of pillar displacement. Meanwhile, because of the rigidity of silicon, the pillars should be able to bend in the range of the CTF. Therefore, the aspect ratio is the most important parameter in the fabrication of Si-NPs.[18] Scanning electron microscopy (SEM) showed regular arrangement of the Si-NPs (**Figure** 2a) 1,000 and 1,400 nm apart (**Figure** 2b). The diameter of the nanopillars was 304 ± 4 nm (n = 40) and normally distributed (**Figure** 2c). The length of each pillar was 2926 ± 55 nm (n=10) (**Figure** 2d and e). The aspect ratio of the Si-NPs was extremely high at almost 10:1, which enabled precise measurements. Because cells constantly interact with their physical environment, any alteration in the nanotopographies of the culture substrate,[19] such as porous morphology,[20] nanopillars,[21] microgrooves,[22] and nanopatterns, will impact cell behavior and gene regulation compared with the plane substrate.[23] The special nanotopography of Si-NPs also affects cellular function. However, the relationship between nanotopography and CTF assessment has not been debated. Conditions other than changes in nanotopography should be controlled to investigate how nanotopography affects cells. We therefore measured CTF in cultured cells on Si-NPs with the same nanotopography to avoid any effects of a difference in the shear modulus between the overall array and bulk material.[16]

2.2. Biocompatibility assessment of Si-NP

Chondrocytes are the only cell type in cartilage tissue. Primary chondrocytes are more closely associated with physiological conditions than cell lines. Therefore, primary chondrocytes that easily degrade *in vitro* were harvested from murine articular cartilage (**Figure** S1). We used o only the first and second passages to maintain the phenotypes.[24] Silicon is a popular biomaterial with excellent biocompatibility *in vitro* and *in vivo*.[25] Nonetheless, the biocompatibility of Si-NPs with chondrocytes should firstly be verified before considering long-term culture. Therefore, we assessed the growth status of chondrocytes cultured on the Si-NPs. We found that the chondrocytes thrived on the Si-NPs, most were distributed individually (**Figure** 2f), and that the growth status resembled that of chondrocytes cultured on bare silicon wafers (**Figure** S2). We then immersed Si-NPs in cell culture medium for 3 days to prepare leaching liquor. We then stained the Si-NPs for calcein-AM/PI, and assayed CCK-8 on days 1, 2, and 3 to assess biocompatibility and found that cell growth did not significantly differ (**Figure** 2g and h). Thus, the Si-NPs did not significantly affect the growth status of chondrocytes, and CTF measured by Si-NPs was reliable. These findings confirmed that Si is appropriate for fabricating NPs to assess chondrocyte CTF.
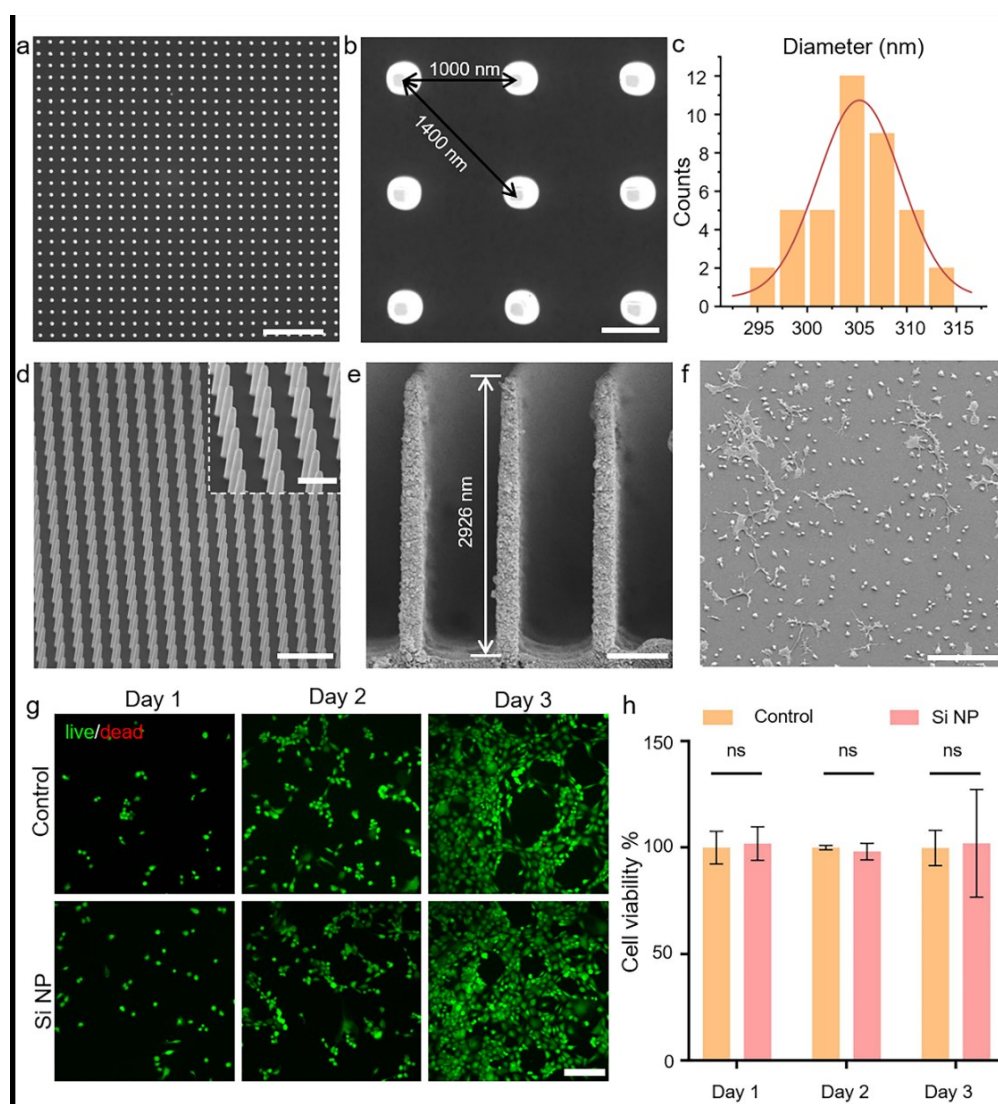
Figure 2. Characterization of Si-NP. (a) Top view of the Si-NP (scale bar, 5 µm). (b) Magnified view of the Si-NP (scale bar, 500 nm). (c) Distribution map of pillar diameter (n = 40). (d) Si-NP from 45° view of Si-NP (scale bar, 3 µm for the overview and 1 µm for the magnified view). (e) Side view of Si-NP (scale bar, 600 nm). (f) Top view of chondrocytes seeded on the Si-NP (scale bar, 200 µm). (g) Calcein-AM/PI staining of chondrocytes cultured with leaching liquor (scale bar, 200 µm). (h) Normalized cell viability cultured with leaching liquor (n = 3). Data presented as mean ± S.D. ns, no significant differences, $P > 0.05$ by two tailed T-test.

2.3. Assessment of CTF in response to OA

8

A relationship between the displacement of the top of the nanopillars and the CTF should be established to validate how the chondrocyte CTF responds to OA. Nanotopographies in a microfabricated substrate might alter the shear modulus between the overall array and bulk material, which is determined by the aspect ratio and surface coverage of the pillars.[22, 26] Although this might occur in the overall array, we quantified CTF based on a single pillar, which can be regarded as a bulk material, using a COMSOL simulation for finite element analysis (**Figure** 3a). Displacement has a linear relationship with CTF within the range of 0 to 10 μN, The linear fits were CTF (μN) = 0.00639 (μN/nm) × displacement (nm) **(Figure** S3). Proinflammatory interleukin (IL)-1β is universally accepted as a model with which to mimic OA *in vitro*[27] as it induces a downstream inflammatory cascade and the onset of mechanical destruction.[28] Therefore, we mimicked OA pathological conditions using IL-1β. Numerous inflammatory mediators are expressed to promote inflammation in response to IL-1β. Nitric oxide (NO) is a catabolic factor that is produced by activated iNOS signaling. Nitric oxide, together with its redox reactions, contributes to perpetuation of OA, and its levels reflect the extent of inflammation.[29] The concentration of NO in the supernatant was significantly increased after incubation with 10 ng/mL IL-1β, indicating that the OA model was established *in vitro* (**Figure** 3b). The NO level was slightly lower than that previously reported because we used 24-, instead of 6-well culture plates. We reduced the seeding density to ensure that most cells were distributed independently of the Si-NPs, [30] then evaluated the CTF of chondrocytes in response to OA. The SEM images showed that the nanopillars bent under the pulling force of chondrocytes in both groups and the displacement of nanopillars was relatively lower in IL-1β, than the control group (**Figure** 3c). Because the numbers of stretched pillars differed and all CTF was in different directions, CTF could not be simply calculated as the sum of all pillars. Therefore, the average CTF of all pillars was taken to represent the CTF. Each cell included 5–27 visible nanopillars (n = 10). The statistical findings suggested that chondrocyte CTF significantly decreased in response to OA. The average displacement and average CTF of individual cells were respectively, 886.7 ± 48.2 nm and 5.7 ± 0.3 μN and 563.9 ± 45.4 nm and 3.6 ± 0.3 μN in the control and experimental group (**Figure** 3d). Our results showed that OA chondrocytes spontaneously participated in the destruction of cytomechanical homeostasis based on CTF degradation. Others have found CTF in the nN range,[31] whereas it was in the μN range in the present study. Therefore, we believe that our results are reliable. This is because silicon is stronger

than organic materials, and therefore avoids self-elongation and substrate interference.[15] Furthermore, CTF is also in the µN range when nanopillars are based on inorganic materials such as quartz[32] and GaN;[33] thus substrate rigidity might have caused a cellular biomechanical response.[34]
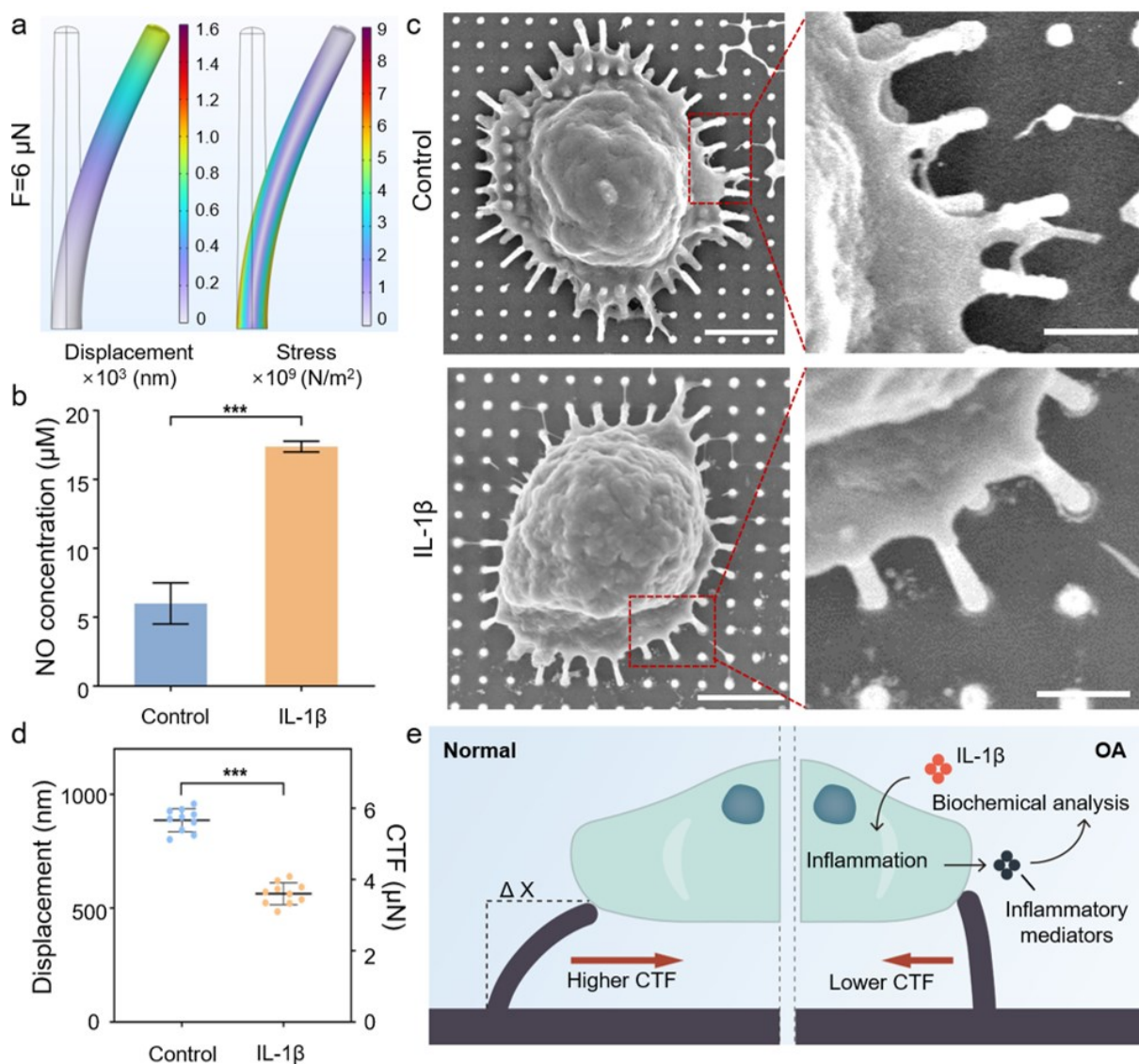

Figure 3. CTF degradation in response to OA. (a) COMSOL simulation of silicon nanopillar. (b) Statistic analysis of the NO expression in supernatant (n = 3). (c) SEM image of normal and IL-1β induced chondrocytes (Scale bar, 3 µm for the overview and 1 µm for the magnified view). (d) Statistic analysis of mean pillar displacement and CTF (n = 10). Data presented as mean ± S.D. ***P < 0.001 by two tailed T-test.

WILEY-VCH

2.4. Mechanism of CTF variation in response to OA

After validating that the CTF of chondrocytes becomes degraded in response to OA, the underlying mechanism for this degradation remains to be addressed. Cell traction force is a mechanical property generated by nuclear-mediated FA assembly and F-actin cytoskeleton polymerization, which is a positive response to the surrounding environment.[10] Therefore, analysis of FA and F-actin in response to OA is essential to clarify CTF degradation in OA. We visualized and quantified FA and F-actin at the single-cell level by immunofluorescence staining (n = 20; **Figure** 4a). The intensity of immunofluorescence emitted by F-actin did not significantly differ (**Figure** 4b), but the distribution of F-actin was not homogeneous. Interleukin-1β elevated the intensity of F-actin fluorescence in chondrocytes.[35] We considered that this was due to higher magnification in our study. The side with lower intensity might have been neglected under low magnification, resulting in a higher statistical average F-actin intensity. As a link between the F-actin cytoskeleton and ECM, FA is responsible for transmitting force to the ECM, and CTF is directly exerted on the ECM through FA. Therefore, the area and counts of FA affect the efficacy of the force generated by F-actin on the ECM and regulate CTF.[36] Vinculin was stained to represent the dynamics of FA because it is a major component of FA that regulates FA dynamics.[37] The mean (**Figure** 4c) and total (**Figure** 4d) area (**Figure** S4) counts of FAs in chondrocytes did not significantly differ in OA. The results of the FA assessment indicated no differences in the force transmission efficiency of OA. Both F-actin expression and structure lead to force generation. F-actin expression did not differ in OA, but its arrangement did. Therefore, we suspect that F-actin reorganization caused this CTF discrepancy.

Compared with the control group, F-actin aggregated at one side of the periphery of the cell, and clutter was distributed (**Figure** 4a), suggesting structural F-actin reorganization.[38] Ras family homolog A and its downstream effector, ROCK participate in regulation of the behavior and fate of cells through cytoskeletal modifications, including contraction, F-actin polymerization, and actomyosin assembly.[39] Activation of the RhoA/ROCK signaling pathway is associated with OA and activation during early OA leads to chondrocyte degradation and hypermechanosensitivity *via* cytoskeletal alterations.[40] Inhibiting RhoA/ROCK can alleviate OA *in vitro* and *in vivo*.[41] Therefore, we assessed the role of

RhoA/ROCK in CTF degradation in patients with OA. We inhibited RhoA/ROCK using Y-27632 and found that F-actin and FA expression decreased, F-actin was distributed (**Figure** 4a), and the CTF significantly recovered (**Figure** 4e). Although CTF was still lower in OA than in the control group, it might hav been because FA and F-actin expression decreased after the RhoA/ROCK signaling pathway was inhibited. Our results implied that F-actin reorganization due to activation of the RhoA/ROCK signaling pathway accounted for CTF degradation in response to OA (**Figure** 4f).
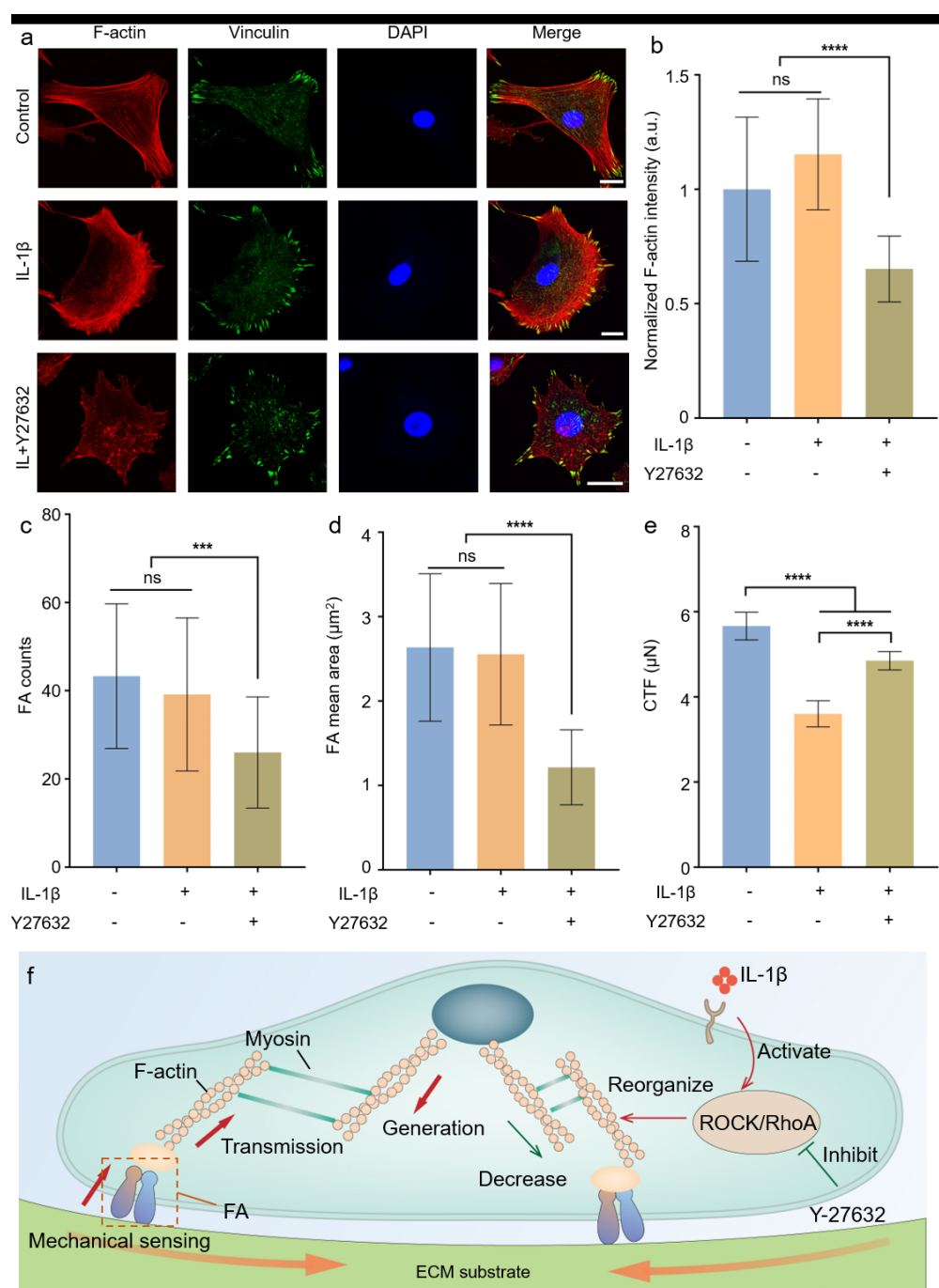
Figure 4. RhoA/ROCK mediated F-actin reorganization is associated with CTF degradation in response to OA. (a) Confocal images of F-actin, Vinculin and DAPI of single chondrocyte the merged images (scale bar, 200 µm). (b) Statistical analysis of normalized F-actin intensity (n = 20). (c) Statistical analysis of FA counts (n = 20). (d) Statistical analysis of FA mean area (n = 20). (e) Statistical analysis of the CTF (n = 10). (f) Schematic illustration of mechanism of CTF degradation in response to OA. Data presented

as mean ± S.D. ns, no significant differences, $P > 0.05$; ***$P < 0.001$; ****$P < 0.0001$ by one-way ANOVA with Tukey post-hoc test.

2.5 Si-NP for drug screening in OA based on Mechanopharmacology

Various methods have been developed for drug screening *in vitro*, including 2D cell culture, organ-on-a-chip, and organoids etc.[42] Though the pharmacological efficiency of numerous drug candidates have been validated *in vitro* using these methods, only a few are clinically applicable. This phenomenon can be attributed to drug kinetics, toxicity, and other factors.[43] However, some drugs that are promising *in vitro* are ineffective *in vivo*, which exacerbates the burden of drug development and screening. Mechanopharmacology has been proposed to evaluate and screen potential drugs. This is because the mechanical environment of a tissue affects the drug pharmacology, mainly at the tissue and organ levels, and the pharmacological effect of drugs on cytomechanics is at the cellular level. Collectively, these two features affect drug efficiency.[44] Therefore, a simple biochemical assessment for drug screening and evaluating efficiency *in vitro* is insufficient. Together with an assessment of mechanopharmacology, a comprehensive understanding of drug efficiency can be obtained. Current drugs for treating OA are mainly anti-inflammatory and pain-relieving, and are limited. Here, we assessed the mechanopharmacology of three clinical drugs with different targets: the COX inhibitor ibuprofen, the IL-1β inhibitor diacerein and the glucocorticoid, dexamethasone (**Figure** 5a). We measured CTF using SEM images and traction force heatmaps of the groups (n = 10) (**Figure** 5b and S5). The CTF significantly recovered after treatment with these drugs, but none recovered to the initial state (**Figure** 5c). However, NO expression did not differ between control chondrocytes and those treated with ibuprofen and dexamethasone (**Figure** 5d). These results indicated that the efficiency of drugs in alleviating biochemical inflammation was not always consistent with their mechanopharmacological efficiency. Therefore, CTF might serve as a complementary biomechanical parameter for OA diagnosis. Meanwhile, the pharmacological responses of hydromechanics can be evaluated based on Si-NPs using high-

throughput screening. Therefore, our device has potential as a mechanopharmacological assessment platform for OA drug screening.
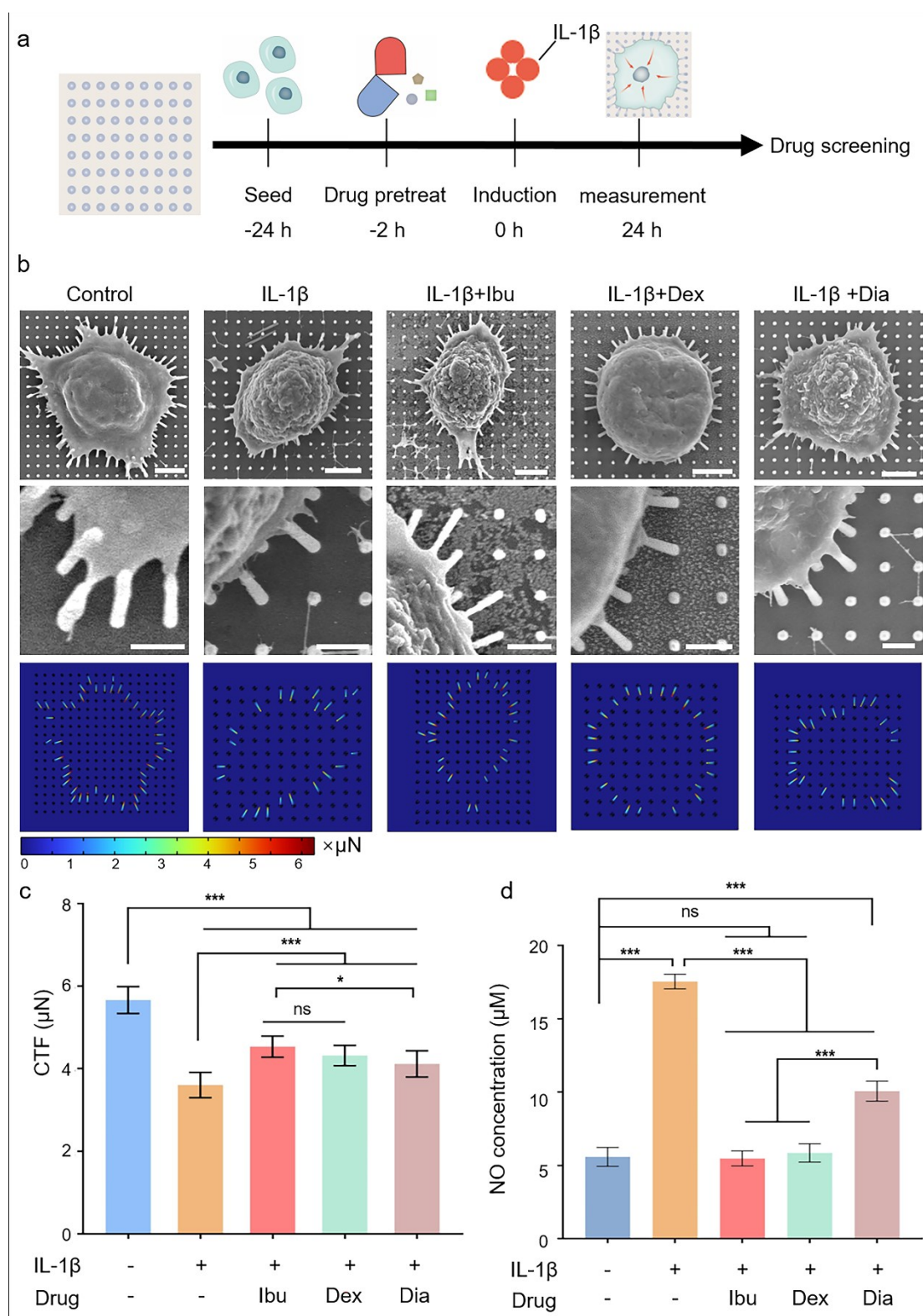
WILEY-VCH

Figure 5. Assessment of CTF for drug screening in OA based on mechanopharmacology. (a) Schematic illustration of the procedure of drug screening. (b) SEM images and heatmap of the CTF treated with ibuprofen, dexamethasone and diacerein respectively (Scale bar, 3 μm for the overview, 1 μm for the magnified view). (c) Statistic analysis of the CTF treated by different drugs (n = 10). (d) Statistic analysis of the NO expression in supernatant treated with different drugs (n = 3). Data presented as mean ± S.D. ns, no significant differences, $P > 0.05$; *$P < 0.05$; ***$P < 0.001$ by one-way ANOVA with Tukey post-hoc test.

3. Conclusion

In this study, a Si-NP was fabricated for CTF assessment with high resolution and good biocompatibility. Based on the Si-NP, we found the CTF degradation in OA was attributed to the F-actin reorganization induced by the activation of RhoA/ROCK signaling pathway. Treated with different drugs, the Si-NP can evaluate the mechanopharmacological efficiency in OA. There were some limitations in our study. First, our chondrocytes were harvested from murine articular cartilage, and the OA cell model was induced by proinflammatory cytokines, which was not the same as cells of OA patients. Second, a further understanding of FA and F-actin in mechanotransduction process of OA should be discovered. Third, more drugs should be taken into discussion to verify its drug screening efficiency adequately. In summary, by assessing CTF based on the Si-NP, this study provided a deeper understanding of the cytomechanical homeostasis destruction in OA and may help us to better understand the process that leads to cartilage erosion and the development of OA at the cellular level. Furthermore, Si-NP showed its potential as the mechanopharmacological platform for drug screening.

4. Experimental Section

Reagent and antibodies: Recombinant murine IL-1β (211-11B) was purchased from PeproTech (NJ, USA). Fetal bovine serum (FBS) (10100147) and collagenase type Ⅱ(17101015) were obtained from Gibco (Shanghai, China). Nitric Oxide assay kit (S0021), Triton X-100 (ST795) and DMSO (ST038) were purchased from Beyotime biotechnology (Shanghai, China). Ibuprofen (V900344) was purchased from Sigma-Aldrich (MO, USA). Diacerein (D102099) was purchased from Shanghai Aladdin Bio-Chem

17

WILEY-VCH

Technology Co., LTD (Shanghai, China). Dulbecco's modified Eagle medium (DMEM) high glucose (11995), phosphate buffered solution (PBS) (P1022), Trypsin-EDTA solution (T1300), Penicillin-Streptomycin liquid (P1400), Dexamethasone (D8040), DAPI resolution (C0060), cell counting kit-8 (CCK-8) (CA1210), Calcein-AM/PI (CA1630), and normal goat serum (SL038) were purchased from Beijing Solarbio Technology Co., Ltd (Beijing, China). Y-27632-2HCl (S1049) was obtained from Selleck Chemicals (Shanghai, China). Anti-Vinculin antibody (ab129002), Goat Anti-Rabbit IgG H&L (Alexa Fluor® 488) (ab150077) and Phalloidin-iFluor 594 Reagent (ab176757) were purchased from Abcam (MA USA).

Si-NP fabrication: The fabrication of Si-NP was followed our previous reported method.[45] In brief, the Si wafer was coated with photoresist after rinsing several times. Subsequently, EBL was applied to fabricate the preliminary array and the Ni was coated on the wafer with the preliminary array. Then removed the photoresist and left a cylinder array with Ni tops. Finally, the Bosch process was used for chemical etching, and removed the Ni tops with a mixture of sulfuric acid, hydrogen peroxide, and deionized water.

Primary mouse chondrocyte isolation and culture: C57/BL6N mice were purchased from Beijing Vital River Biotechnology, Beijing, China. All animal handling procedures were performed under the supervision of Committee on Ethics of Beijing Institute of Nanoenergy and Nanosystems (A-2022067). Primary chondrocyte isolation was performed according to the previously reported method.[24] Briefly, the 1-week-old C57/BL6N mouse were sacrificed after deep anesthesia. Then the articular cartilage was obtained from knee joints. Soft tissues were removed carefully under microscope. Then digested the articular cartilage with 0.25% Trypsin-EDTA solution at 37°C in a 5% CO_2 incubator for 45 minutes to remove residual soft tissues. After 45 minutes digestion, washed the articular cartilage with 1 × PBS for 3 times. Then minced into small pieces and digested by 0.2 % w/v type II collagenase for 4 hours to release chondrocytes. Digested suspension was filtered through a 70 μm strainer. After a 5 min 1200 rpm centrifugation, discarded the supernatant and resuspended with cell culture medium, which was DMEM high glucose supplemented with 10 % fetal bovine serum (FBS) and 1 % Penicillin-Streptomycin. Then plated into culture dishes and incubated at 37 °C, 5 % CO_2. Passaged at 80 %-90 % confluency. Only the first and second passages of chondrocytes were used for the experiment to avoid phenotype degradation.

Biocompatibility evaluation: The biocompatibility of Si-NP was measured by Calcein-AM/PI cell staining and CCK-8 test for day 1, day 2, day 3. Leaching liquor was collected by immersing with cell culture medium for 72 h. Chondrocytes were incubated for 24 h before measurement. Then removed the culture medium by the leaching liquor and incubated at 37 ℃ for 24 h, 48 h, 72 h respectively. The live/dead cell staining and CCK-8 test were carried out according to the manufacturer's protocol.

Osteoarthritic chondrocytes induction: Chondrocytes were cultured in a 24-well plate stimulated with 10 ng/mL murine IL-1β to induce osteoarthritic inflammation. Y-27632-2HCl was used to inhibit RhoA/ROCK signaling pathway at a concentration of 10 μM. 10^{-6} M Dexamethasone, 500 mM Ibuprofen, and 10 μM Diacerein were used for anti-inflammation respectively. The supernatant was collected to measure the expression of NO using NO assay kit following manufacturer instructions.

CTF assessment: Wafer with Si-NP array was sterilized with 75 % ethanol and UA irradiation before culturing. The wafer was placed in the 24-well culture plate and chondrocytes were seeded for 24 h prior to intervention. Cells on the Si-NPs were fixed with 4 % paraformaldehyde for 20 min and then rinsed with PBS for three times. Then dehydrated with gradient alcohol (50 %, 60 %, 70 %, 80 %, 85 %, 90 %, 95 %, 100 % v/v %) for 15 min each sequentially. The sample was observed under scanning electron microscope (SEM) (SU8020, Hitachi). The CTF was detected by measuring the displacement of the tip of each pillar by Image J (National Institutes of Health, Bethesda, MD, USA). The finite element simulation (FEM) was performed by COMSOL multiphysics software (COMSOL Burlington, MA, USA) to establish the association between displacement and applied CTF. According our previous report,[45b] the mechanical properties of silicon were as indicated below: Young's modulus E = 150 GPa, Poisson's ratio = 0.278, and the density ρ = 2330 kg/m^3. Characterized by SEM, the nanowire has a shape with a length of 2926 ± 55 nm (n = 10) and diameter of 304 ± 4 nm (n = 40). The lateral and diagonal distances between two nanopillars are 1000 nm and 1400 nm respectively.

Immunofluorescent staining: Chondrocytes were plated on glass-bottom 35 mm dishes for immunofluorescent staining and confocal imaging. Briefly, cells were fixed with 4 % paraformaldehyde for 20 min and permeabilized with 0.3 % Triton X-100 for 10 min at room temperature followed by blocking with 5 % normal goat serum for 45 min. Afterwards, vinculin was stained with rabbit monoclonal to vinculin primary antibody (1:150) overnight followed by incubated with goat anti-rabbit

WILEY-VCH

IgG H&L Alexa Fluor® 488-conjugated secondary antibody (1:1000) for 1 h. F-actin was stained with Phalloidin-iFluor 594 for 45 min and the nuclear was stained with DAPI solution. Images were captured by confocal fluorescence microscope (Leica SP8). Image J was used to F-actin and FA quantification according to the literature.[36]

Statistical analysis: All experiments were repeated at least three times. Statistical analysis was performed using GraphPad Prism version 8.0. All data were displayed as mean ± standard deviation (S.D). Two groups were compared using two tailed T-test. Multigroup comparison was performed by one-way analysis of variance (ANOVA) with Tukey post-hoc test. The difference was significant when P value < 0.05. The P value was defined as ns > 0.05, *< 0.05 , **< 0.01, ***< 0.001, ****< 0.0001.

Supporting Information

Supporting Information is available from the Wiley Online Library or from the author.

Acknowledgements

Conflict of Interest

WILEY-VCH

The authors declare no conflict of interest.

Data Availability Statement

The data that support the findings of this study are available from the corresponding author upon reasonable request.

References

[1] a) J. N. Katz, K. R. Arant, R. F. Loeser, *JAMA* **2021**, 325, 568; b) A. Litwic, M. H. Edwards, E. M. Dennison, C. Cooper, *Brit Med Bull* **2013**, 105, 185.

[2] J. G. Quicke, P. G. Conaghan, N. Corp, G. Peat, *Osteoarthr Cartilage* **2022**, 30, 196.

[3] S. Glyn-Jones, A. J. R. Palmer, R. Agricola, A. J. Price, T. L. Vincent, H. Weinans, A. J. Carr, *The Lancet* **2015**, 386, 376.

[4] D. J. Hunter, D. Schofield, E. Callander, *Nat Rev Rheumatol* **2014**, 10, 437.

[5] A. Mahmoudian, L. S. Lohmander, A. Mobasheri, M. Englund, F. P. Luyten, *Nat Rev Rheumatol* **2021**, 17, 621.

[6] J. Martel-Pelletier, A. J. Barr, F. M. Cicuttini, P. G. Conaghan, C. Cooper, M. B. Goldring, S. R. Goldring, G. Jones, A. J. Teichtahl, J. P. Pelletier, *Nat Rev Dis Primers* **2016**, 2, 16072.

[7] W. H. Robinson, C. M. Lepus, Q. Wang, H. Raghu, R. Mao, T. M. Lindstrom, J. Sokolove, *Nat Rev Rheumatol* **2016**, 12, 580.

WILEY-VCH

[8] J. D. Humphrey, E. R. Dufresne, M. A. Schwartz, *Nat Rev Mol Cell Bio* **2014**, 15, 802.

[9] A. D. Theocharis, S. S. Skandalis, C. Gialeli, N. K. Karamanos, *Adv Drug Deliver Rev* **2016**, 97, 4.

[10] A. Elosegui-Artola, X. Trepat, P. Roca-Cusachs, *Trends Cell Biol* **2018**, 28, 356.

[11] M. Maurer, J. Lammerding, *Annu Rev Biomed Eng* **2019**, 21, 443.

[12] a) Z. Liu, X. Cui, Y. Fan, Z. Li, *Innovation* **2022**, 3, 100313; b) X. Wan, Z. Liu, L. Li, *Adv Funct Mater* **2021**, 31.

[13] a) P. Lu, K. Takai, V. M. Weaver, Z. Werb, *CSH Perspect Biol* **2011**, 3; b) M. Kapoor, J. Martel-Pelletier, D. Lajeunesse, J. P. Pelletier, H. Fahmi, *Nat Rev Rheumatol* **2011**, 7, 33.

[14] S. G. Higgins, M. Becce, A. Belessiotis-Richards, H. Seong, J. E. Sero, M. M. Stevens, *Adv Mater* **2020**, 32, e1903862.

[15] Z. Li, J. Song, G. Mantini, M. Y. Lu, H. Fang, C. Falconi, L. J. Chen, Z. L. Wang, *Nano Lett* **2009**, 9, 3575.

[16] D. W. Zhou, M. A. Fernandez-Yague, E. N. Holland, A. F. Garcia, N. S. Castro, E. B. O'Neill, J. Eyckmans, C. S. Chen, J. Fu, D. D. Schlaepfer, A. J. Garcia, *Nat Commun* **2021**, 12, 2359.

[17] S. Ghassemi, G. Meacci, S. Liu, A. A. Gondarenko, A. Mathur, P. Roca-Cusachs, M. P. Sheetz, J. Hone, *P Natl Acad Sci USA* **2012**, 109, 5328.

[18] J. Y. Shiu, L. Aires, Z. Lin, V. Vogel, *Nat Cell Biol* **2018**, 20, 262.

[19] K. Anselme, N. T. Wakhloo, P. Rougerie, L. Pieuchot, *Adv Healthc Mater* **2018**, 7, e1701154.

[20] M. Risbud, J. Ringe, R. Bhonde, M. Sittinger, *Cell Transplant* **2001**, 10, 755.

[21] C. R. Pedrosa, D. Arl, P. Grysan, I. Khan, S. Durrieu, S. Krishnamoorthy, M. C. Durrieu, *ACS Appl. Mater. Interfaces* **2019**, 11, 8858.

[22] E. Huethorst, M. F. Cutiongco, F. A. Campbell, A. Saeed, R. Love, P. M. Reynolds, M. J. Dalby, N. Gadegaard, *Biofabrication* **2020**, 12, 025009.

[23] S. S. Han, M. O. Cho, K. M. Huh, S. W. Kang, *RSC Adv* **2020**, 11, 39.

[24] M. Gosset, F. Berenbaum, S. Thirion, C. Jacques, *Nat Protoc* **2008**, 3, 1253.

[25] R. R. Castillo, M. Vallet-Regí, *Int J Mol Sci* **2019**, 20.

[26] C. H. Rasmussen, P. M. Reynolds, D. R. Petersen, M. Hansson, R. M. McMeeking, M. Dufva, N. Gadegaard, *Adv Funct Mater* **2016**, 26, 815.

[27] C. I. Johnson, D. J. Argyle, D. N. Clements, *Vet J* **2016**, 209, 40.

[28] a) Z. Jenei-Lanzl, A. Meurer, F. Zaucke, *Cell Signal* **2019**, 53, 212; b) Y. Deng, J. Lu, W. Li, A. Wu, X. Zhang, W. Tong, K. K. Ho, L. Qin, H. Song, K. K. Mak, *Nat Commun* **2018**, 9, 4564.

[29] S. B. Abramson, *Osteoarthritis and Cartilage* **2008**, 16, S15.

[30] S. Zhou, J. Shi, H. Wen, W. Xie, X. Han, H. Li, *Food Funct* **2020**, 11, 7935.

[31] J. Fu, Y. K. Wang, M. T. Yang, R. A. Desai, X. Yu, Z. Liu, C. S. Chen, *Nat Methods* **2010**, 7, 733.

[32] D. J. Kim, G. S. Kim, J. H. Hyung, W. Y. Lee, C. H. Hong, S. K. Lee, *Nanoscale Res Lett* **2013**, 8, 332.

[33] Q. Zheng, M. Peng, Z. Liu, S. Li, R. Han, H. Ouyang, Y. Fan, C. Pan, W. Hu, J. Zhai, Z. Li, Z. L. Wang, *Sci Adv* **2021**, 7.

[34] H. Wolfenson, B. Yang, M. P. Sheetz, *Annu Rev Physiol* **2019**, 81, 585.

[35] a) R. Li, X. Song, G. Li, Z. Hu, L. Sun, C. Chen, L. Yang, *ACTA BIOCH BIOPH SIN* **2019**, 51, 1026; b) S. Pritchard, F. Guilak, *Arthritis Rheum* **2006**, 54, 2164.

[36] G. Nardone, J. Oliver-De La Cruz, J. Vrbsky, C. Martini, J. Pribyl, P. Skladal, M. Pesl, G. Caluori, S. Pagliari, F. Martino, Z. Maceckova, M. Hajduch, A. Sanz-Garcia, N. M. Pugno, G. B. Stokin, G. Forte, *Nat Commun* **2017**, 8, 15321.

[37] a) C. Grashoff, B. D. Hoffman, M. D. Brenner, R. Zhou, M. Parsons, M. T. Yang, M. A. McLean, S. G. Sligar, C. S. Chen, T. Ha, M. A. Schwartz, *Nature* **2010**, 466, 263; b) S. V. Plotnikov, A. M. Pasapera, B. Sabass, C. M. Waterman, *Cell* **2012**, 151, 1513.

WILEY-VCH

[38] C. Zhou, M. Duan, D. Guo, X. Du, D. Zhang, J. Xie, *Int J Oral Sci* **2022**, 14, 15.

[39] R. El Masri, J. Delon, *Nat Rev Immunol* **2021**, 21, 499.

[40] Z. Deng, Y. Jia, H. Liu, M. He, Y. Yang, W. Xiao, Y. Li, *Am J Transl Res* **2019**, 11, 5324.

[41] A. Rodríguez-Trillo, C. Pena, S. García, E. Pérez-Pampín, M. Rodríguez-López, A. Mera-Varela, A. González, C. Conde, *Front Immunol* **2022**, 13.

[42] a) L. Ren, X. Zhou, R. Nasiri, J. Fang, X. Jiang, C. Wang, M. Qu, H. Ling, Y. Chen, Y. Xue, M. C. Hartel, P. Tebon, S. Zhang, H. J. Kim, X. Yuan, A. Shamloo, M. R. Dokmeci, S. Li, A. Khademhosseini, S. Ahadian, W. Sun, *Small Methods* **2020**, 4; b) Y. Li, E. Kumacheva, *Sci Adv* **2018**, 4, eaas8998; c) J. Nie, Q. Gao, J. Fu, Y. He, *Adv Healthc Mater* **2020**, 9, e1901773; d) Y. Ling, W. Zhang, P. Wang, W. Xie, W. Yang, D.-A. Wang, C. Fan, *Bioact Mater* **2021**, 6, 2914.

[43] A. Mansinho, V. Boni, M. Miguel, E. Calvo, *Ann Oncol* **2019**, 30, 1460.

[44] R. Krishnan, J. A. Park, C. Y. Seow, P. V. Lee, A. G. Stewart, *Trends Pharmacol Sci* **2016**, 37, 87.

[45] a) Y. M. Jin, Y. L. Zhang, H. Ouyang, M. Z. Peng, J. Y. Zhai, Z. Li, *Sensor Mater* **2015**, 27, 1071; b) H. Feng, H. Ouyang, M. Peng, Y. Jin, Y. Zhang, Z. Liu, Y. Zou, C. Zhao, Y. Fan, J. Zhai, Z. L. Wang, Z. Li, *Nano Energy* **2018**, 50, 504.

Direct mapping of cytomechanical homeostasis destruction in osteoarthritis based on silicon nanopillar array

Dengjie Yu, Qingbin Nie, Jiangtao Xue, Ruizeng Luo, Shiwang Xie, Shengyu Chao, Engui Wang, Linlin Xu, Yizhu Shan, Zhuo Liu[*], Yusheng Li[*], Zhou Li[*]
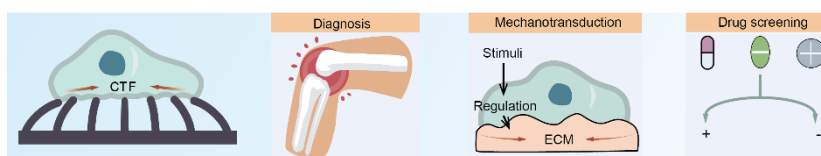
In this study, a silicon nanopillar array (Si-NP) with high spatial resolution and promising mechanical property is fabricated to directly reflect the cytomechanical homeostasis destruction in osteoarthritis (OA) by measuring the cell traction force (CTF), which provides a deeper understanding in the progression of OA. Meanwhile, The Si-NP also shows the potential in disease diagnosis and drug screening from cytomechanical standpoint.